Solidification microstructures in laser welding of dissimilar metals

G. Phanikumar, P. Dutta*, and K. Chattopadhyay+

Department of Metallurgy, *Department of Mechanical Engineering

Indian Institute of Science, Bangalore 560012 INDIA

+corresponding author, email: kamanio@metalrg.iisc.ernet.in

INTRODUCTION

Laser welding offers a high power, high speed clean heat source to join materials of different properties. An understanding of the physical processes that take place during welding that effect the weld material properties exists. However, laser welding of dissimilar metals has not been studied in detail in the literature [1,2]. The majority of this literature is concentrated on the joining of dissimilar steels and deal with the analysis of the problem in a case-by-case manner. Analysis of a dissimilar metal joint offers a number of challenges arising out of complexities such as dissimilar metal properties, asymmetric weld pool shape, mixing of the molten metals, segregation, formation of intermetallic compounds and metastable microstructures. Mathematical modeling and simulation have been used to gain insight into the physical processes that occur in a weld pool [3,4,5], as it is very difficult to make a direct observation of the weld pool solidification behavior [6].

A binary couple of pure metals is simpler to start with to understand the basic issues in dissimilar joints. In a model dissimilar couple, the two metals should have a significant difference in their physical properties so that the main issues are highlighted. However, it is not desirable to choose binary systems with miscibility gaps or intermetallic compounds in it, as it would make the system additionally complex and difficult for a systematic analysis. Copper and nickel have different physical properties [7], and have an isomorphous phase diagram making it an ideal system for study. We present results of our investigation on this system.

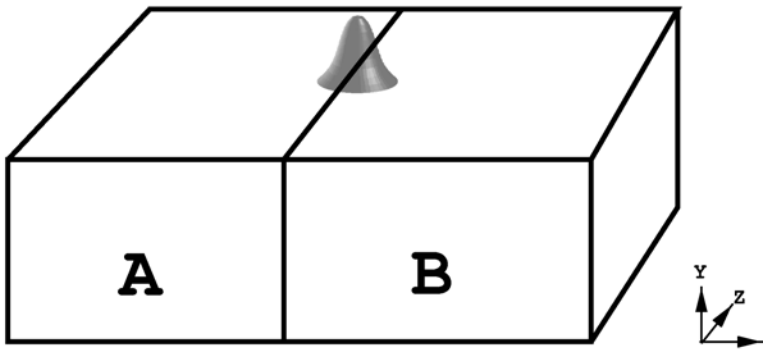

Figure 1. Schematic of Laser welding setup.

EXPERIMENTAL RESULTS

A schematic of the laser welding setup is shown in Fig. 1. Commercial high purity metals are taken in the form of bars of square cross section of 7mm × 7mm each and are fixed on a CNC table in butt-weld geometry. Continuous wave CO_2 laser is used as the heat source with a co-axial inert gas shroud. Weld samples are cut to make transverse sections for characterization using optical microscopy, scanning electron microscopy (SEM) and composition analysis using EDAX.

The weld pool shapes, at low and high laser scan speeds, are shown in figure 2. At high scan speed, the melt pool is a shallow one with an aspect ratio of 2 (figure 2a). At low scan speed, it is a deep and narrow one with depth equal to the thickness of the sample (figure 2b). An asymmetry in the pool shape with more melting of nickel is observed at all scan speeds. Some amount of porosity is also noticed. The microstructure reveals segregation patterns that are asymmetric in nature. At high scan speed, the 'eye' of the pattern lies on the nickel side and at low scan speed, there is one 'eye' towards the top and one towards the bottom.

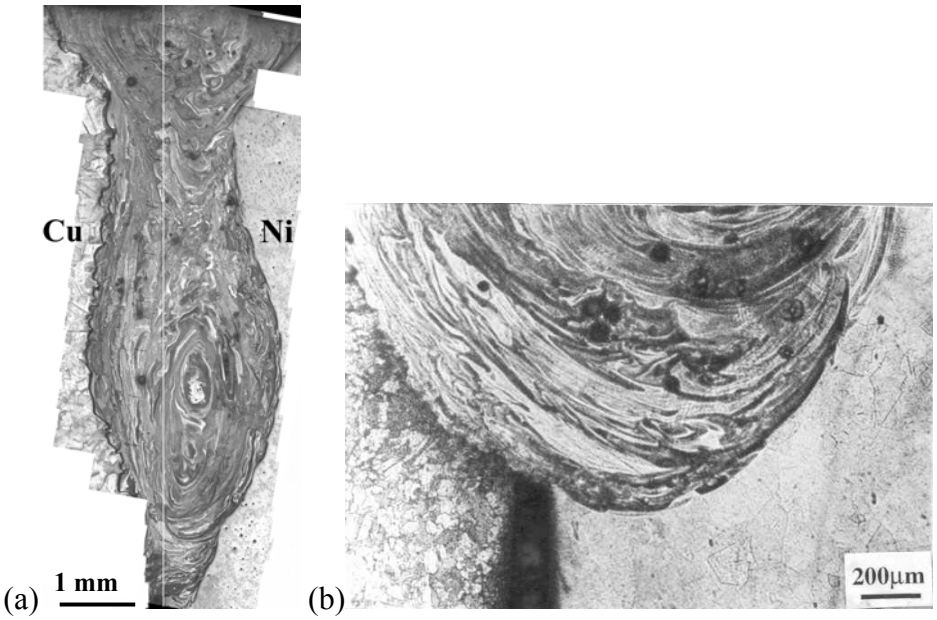

Figure 2. Microstructure of welds at scan speeds of (a) 50mm/s (b)125mm/s.

The asymmetry of the microstructure of the weld interface can be clearly seen at higher magnification. Nickel-weld interface is sharp and shows cellular growth of the base metal in to the weld (figure 3b). Weld microstructure near the interface also shows bands. However, cells extend through these bands. A closer look at the interface (figure 3c) reveals that the weld pool solidifies from the substrate grains expitaxially as in welds of similar metals [8] and after a minute growth, a transition in the growth pattern from planar to cellular is observed. The concentration of copper in the grown solid close to the interface is ~8% copper indicating a sharp change in concentration during the regrowth at the surface melt interface.

On the copper side, we notice the interface to be rough with swirls of copper-rich and nickel-rich regions in an irregular pattern (figure 3a). The exact extent of melting on the copper side is larger than the mixing zone. There is a clear epitaxy between the grains. Copper grains as well as cellular regions which have finger like intrusion are seen at the interface.

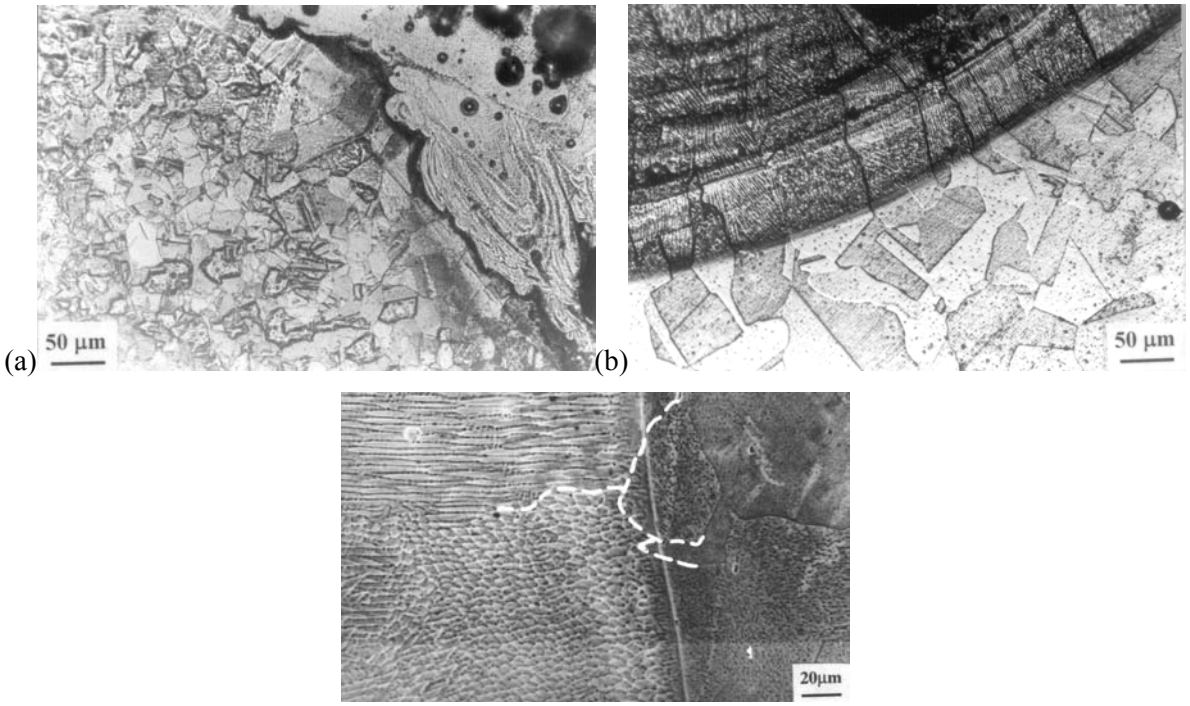

Figure 3. Interface microstructures on (a) copper side and (b) nickel side (c) nickel side, white dotted line shows possible extent of respective substrate grains.

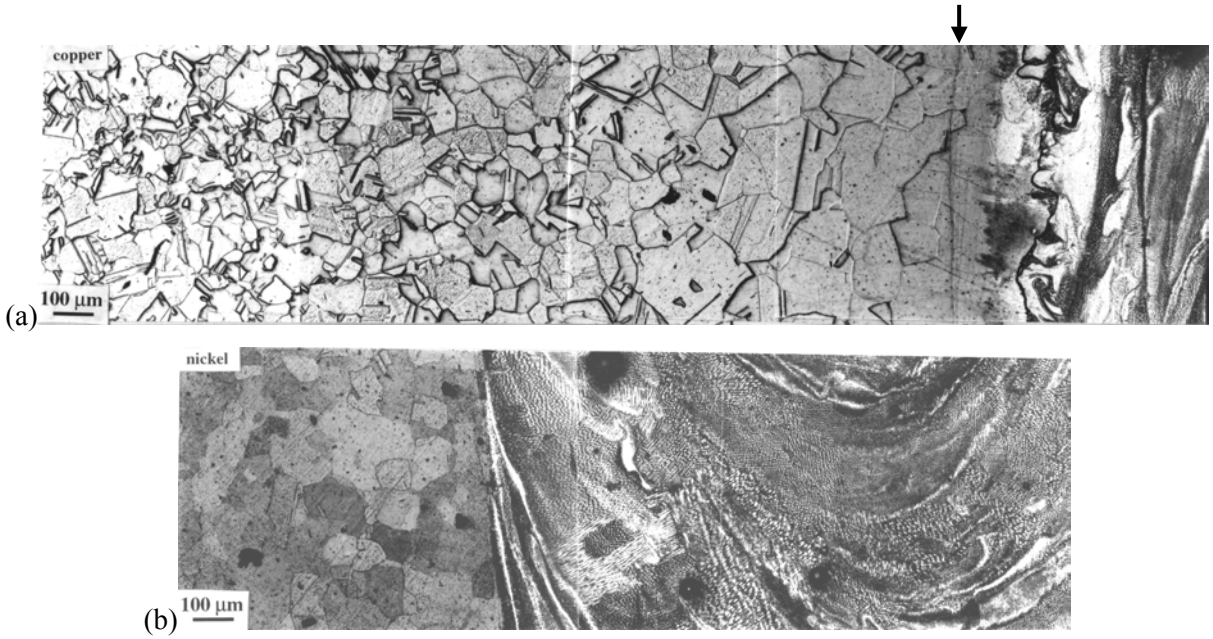

Figure 4 Microstructure on the top view (a) copper side (b) nickel side.

A typical microstructure of the weld pool and the grain structures of the surrounding matrices is shown in the figure 4a. The starting grain size of copper is of the order of 100 µm which can be seen in the parent metal away from the weld pool. The grains are considerably coarsened near the weld pool. The dark line revealing a slightly different etching effect at the weld interface shows the actual extent of fusion. This is also seen in the transverse section (figure 3a). The boundary between mixed weld pool region and the copper matrix is jagged while banded contrast can be seen in weld pool. In contrast, the grain size of the nickel side does not change till the weld pool boundary (figure 3b).

(a) 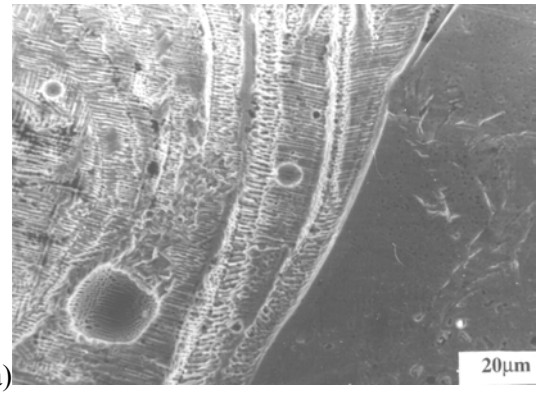

(b) 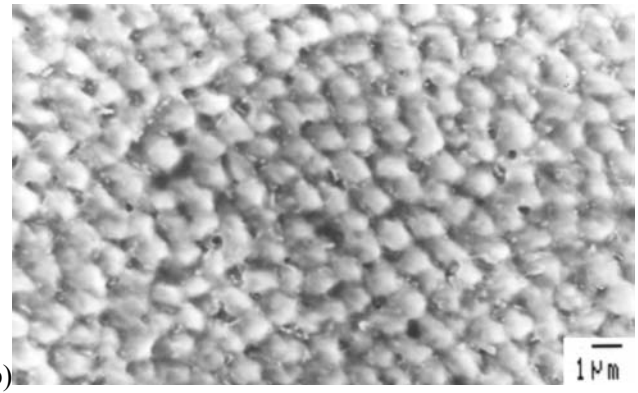

Figure 5. (a) Banded growth of weld region on nickel side. (b) Cellular microstructure in the weld region.

The growth of the solid is not steady and is found to oscillate from a fine scale to a coarse scale with coinciding compositional fluctuations as the growth progresses (figure 5a). In the extreme case, the composition fluctuation in nickel rich side was found to vary from ~4 wt% Cu to ~20 wt%Cu in two adjacent bands with cell free and cellular microstructure respectively, as measured using the EDAX attachment to the SEM. These are termed as low velocity bands by Kurz and coworkers [9]. The microstructure throughout the weld exhibits a cellular/dendritic structure (figure 5). Extensive microstructural banding, compositional fluctuations and irregularity of the microstructural features on copper side are very distinct for all scan speeds. Microstructural bands comprise a change in the scale of microstructure as well as fluctuations in the composition.

As can be seen in figure 4 and 5a, the bands are normal to the solidification direction suggesting an oscillatory rate of growth of solid in to the weld. The presence of such a kind of growth mode is confirmed recently by direct visualization [6]. We observe that the microstructural features discussed above are common to several other dissimilar couples including Al-Ti [10], Fe-Cu and Fe-Ni[11]. The interface on Al side in Ti-Al, Cu side in Fe-Cu, and Ni side on Fe-Ni are jagged with two distinct boundaries of fusion and mixing. The high amount of melting on Al in Ti-Al was attributed to its very low melting point vis-à-vis Ti and Fe in Fe-Cu for its low thermal diffusivity. Convection in the melt pool is speculated as responsible for the banding and mixing zone irregularities. It is not surprising that a majority of the microstructural bands take the shape of convection patterns. We suppose that the convection in the pool and the simultaneous shrinkage of weld pool due to solidification bringing liquid of varying temperatures and compositions near the growth front result in the oscillatory growth responsible for banding. In the next section we try to model the dissimilar welding process in order to gain some insight in to the features described above.

COMPUTATIONAL MODELLING

A full scale modeling of a moving dissimilar weld pool (i.e. produced by a continuous laser welding) requires modeling of the melting, mixing and solidification at both micro and macro scales. Solidification modeling in such a situation is a very difficult task, since the composition can vary sharply at any location. In addition, the solidification process would depend on the scale of mixing of the two metals at the interface, which may be very difficult to determine using present modeling tools. In the present case, we attempt to model the melting and mixing processes at a macroscopic level. The objective is to study the asymmetry of a weld pool caused by a symmetric heat source on a dissimilar metal joint and the associated temperature, velocity and mass fraction distributions.

Mathematical Formulation

A schematic of the computational domain used for numerical simulation is shown in Fig 1a. Two pieces of copper and nickel with equal dimensions are kept in a butt joint. A Gaussian heat input is applied from the top at the centerline of the butt joint such that the heat is distributed equally on both pieces. The fluid motion in the melt pool is assumed to be laminar and incompressible with Boussinesq approximation. The top surface after melting is assumed flat. Thermophysical properties are taken to be different for solid and liquid metals, and variation with temperature taken in to consideration using a smooth fit over the data available at different temperatures in the literature [7]. For properties of the mixtures, semi-empirical correlations are used. Phase change is modeled using an enthalpy-porosity technique [12]. In this technique, a parameter ε, which indicates the liquid fraction in a control volume, is used to define the enthalpy of the material continuous across the phase change. The same parameter acts as the porosity term to damp the permeability and thus the fluid velocity to zero in the solid region. The resulting governing equations for mass, momentum, energy and species equations are as follows [13]:

Continuity:

$$\frac{\partial \rho}{\partial t} + \nabla \cdot (\rho U) = 0 \qquad [1]$$

Momentum:

$$\frac{\partial}{\partial t}(\rho u) + \nabla \cdot (\rho U u) = \nabla \cdot (\mu \nabla u) - \frac{\partial p}{\partial x} - \left(\frac{K(1-\varepsilon)^2}{\varepsilon^3 + b} \right) u \qquad [2]$$

$$\frac{\partial}{\partial t}(\rho v) + \nabla \cdot (\rho U v) = \nabla \cdot (\mu \nabla v) - \frac{\partial p}{\partial y} - \left(\frac{K(1-\varepsilon)^2}{\varepsilon^3 + b} \right) v + \rho g [\beta_T (T - T_r) - \beta_C (C - C_r)] \qquad [3]$$

$$\frac{\partial}{\partial t}(\rho w) + \nabla \cdot (\rho U w) = \nabla \cdot (\mu \nabla w) - \frac{\partial p}{\partial z} - \left(\frac{K(1-\varepsilon)^2}{\varepsilon^3 + b} \right) w \qquad [4]$$

Energy:

$$\frac{\partial}{\partial t}(\rho H) + \nabla \cdot (\rho U H) = \nabla \cdot (k \nabla T) - \frac{\partial}{\partial t}(\rho \Delta H) \qquad [5]$$

Mass fraction:

$$\frac{\partial C}{\partial t} + \nabla \cdot (UC) = \nabla \cdot (D_{AB} \nabla C) \qquad [6]$$

Where, μ is viscosity, u,v,w are velocity components along x,y,z, U is the total velocity vector, T is Temperature, σ is surface tension, C is solutal weight fraction, ρ is density, t is time, p is pressure, H is enthalpy, k is thermal conductivity and D_{AB} is solutal diffusivity. K is a morphological constant, b is an arbitrary small number to prevent division by zero, ΔH is the latent heat content of a control volume, and ε is the liquid fraction.

At time $t=0$, the entire domain is in the solid state at room temperature. At time $t>0$, at the top surface of the work piece, a heat flux with a Gaussian distribution is applied symmetric about the centerline. At the flat free surface of the liquid, shear force due to surface tension is applied to take marangoni convection in to account. No mass transfer is considered at the top surface. The bottom surface is insulated, while the four sides are subjected to convective and radiative heat loss.

The three-dimensional coupled continuity, momentum, energy, and mass fraction equations along with the boundary conditions are solved numerically using a finite volume technique. The general framework of the numerical solution rests on the SIMPLER algorithm [12], modified appropriately to

accommodate phase change processes and mixing of dissimilar metals. Transient studies were carried out until some mixing patterns are obtained. The thermophysical data for the case study is given in table-1. A non-uniform grid of 64×48×64 is used to discretize the computational domain, with a high concentration of grids inside the weld pool [15,16].

Discussion of Computational Results

Due to the difference in thermal diffusivity of copper and nickel, heat diffusion in copper will be more than in nickel during the conduction phase of the heating process. The low thermal conductivity of nickel more than compensates for its high melting point and melts first [15]. After nickel starts melting, the weld pool develops a flow starting from the maximum temperature location and moves outwards. Since the temperature coefficient of the surface tension (σ_t) is negative, the fluid in the center is pulled radially outward. From fig. 6, it can be seen that due to asymmetric heating and convection, isotherms bend and become non-circular. On the free surface, convection brings the hot liquid from the maximum temperature location to the edges of the weld pool, thus increasing the width of the weld pool. By continuity, this flow also brings the cold fluid from the bottom of the pool to the surface. The amount of heat transported in the vertical direction is therefore relatively small. Hence, the melt pool tends to be shallow and wide. Since surface tension forces are dominant, the maximum velocity occurs on the free surface and the eye of the convection cell is close to the surface. However, at low scan speeds, keyhole formation with enhanced absorption leads to deep weld pools.

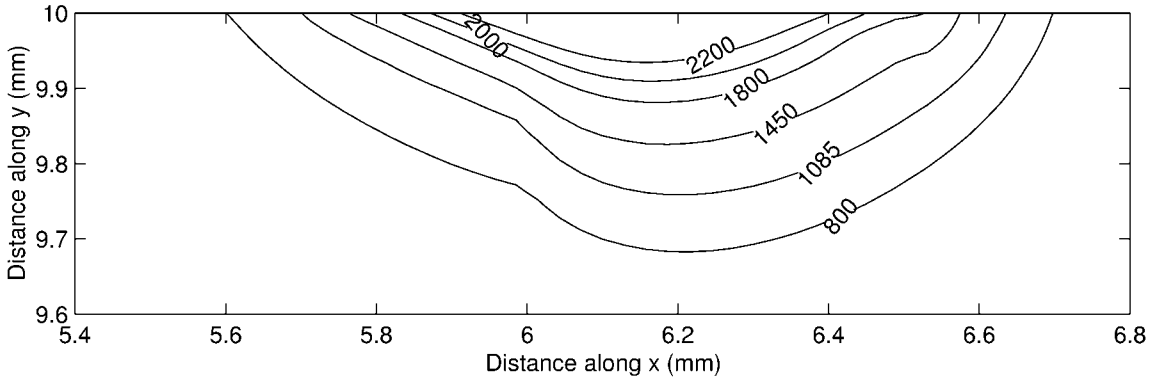

(a)

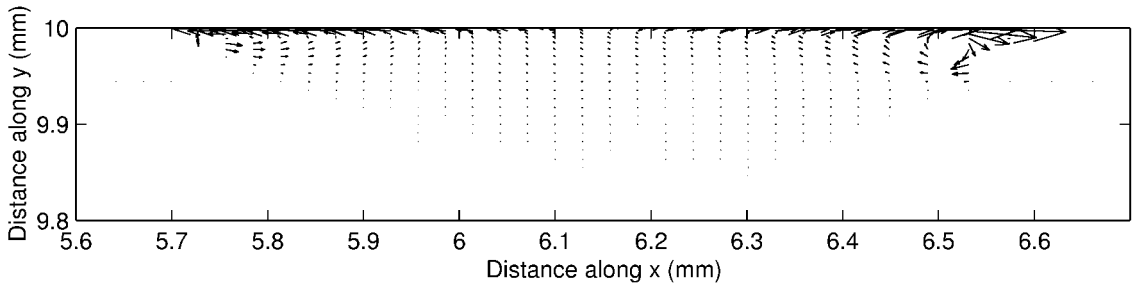

(b)

Figure 6. (a)Temperature contours and (b)velocity profile of the weld region. The laser is centered at (6,10). The properties for the domain are of copper to the left of laser center and of nickel to the right.

It is observed that the nickel side melts first and subsequently convection carries the heat towards the copper side. Thus, the rise in temperature and melting of the copper side is aided by convection from the nickel side, in addition to direct laser heating. This information is not easily obtainable from experiments alone, and hence it is considered an important contribution from the numerical modeling. The final melt pool shape is determined by the convection patterns resulting in an

asymmetric weld pool as also observed in experiments. The temperature gradient on the copper side is low, and the extended heating leads to coarsening of the substrate grains adjacent to weld as also observed in experiments. The large cooling rate ($\sim 5\times10^{5}\, Ks^{-1}$) experienced by the weld region also suggests formation of fine microstructure.

CONCLUSIONS

Laser welding of dissimilar materials consisting of copper-nickel has been studied both experimentally and numerically. The experimental observations reveal several complex features of dissimilar metal welding. There is an asymmetry in the melt pool shape about the centerline of the butt weld even when the heat source is placed symmetrically on either side. Secondly, there is a large difference in microstructural features between the two sides of the metal-weld interface. The higher conductivity metal side has a smooth interface while the other side has a jagged one. Thirdly, in spite of high convection in the melt pool, the weld has inhomogeneity of composition and microstructure with banding. An attempt has been made to computationally model this complex phenomenon. In spite of some simplifying assumptions, the model is able to capture some of the essential features of the process observed experimentally. This work lays a strong foundation for future studies on the complex issues in dissimilar joints.

ACKNOWLEDGEMENTS

The authors acknowledge Prof. J. Mazumder, University of Michigan Ann Arbor, USA, Technical University of Clausthal, Germany and Supercomputing Education and Research Center, Indian Institute of Science, Bangalore, India for their facilities.

TABLE -1. Physical properties of copper and nickel

Property	**Copper**	**Nickel**
Melting Point (^{o}C)	1083	1453
Thermal Conductivity ($Wm^{-1}K^{-1}$)	399	88.5
Specific Heat ($JKgK^{-1}$)	386	452
Density (Kgm^{-3})	8900	7905
Latent Heat ($kJmol^{-1}$)	13.02	17.16

REFERENCES

1. Z. Sun and J.C. Ion, *Journal of Materials Science*, 1995, vol. 30, pp.4205-4214.
2. G. Metzger and R. Lison, *Welding Journal*, 1976, vol. 55, No. 8, pp. 230s-240s.
3. L. Chan, J. Mazumder and M. M. Chen, *Metallurgical Transactions*, vol. 15A, (1984), p. 2175-2184.
4. T. Debroy and S. A. David, *Reviews of Modern Physics*, vol. 67, (1995), p. 85-112.
5. F. K. Chung and P.S. Wei, *Journal of Heat Transfer*, vol. 121, (1999), p. 451-461.
6. P.S. Mohanty and J. Mazumder, *Metallurgical Transactions*, vol. 29B, (1999), p. 1269-1279.
7. Eric A. Brandes, Smithells Metals Reference Book, Sixth Edition, Butterworths & Co Publications Ltd., London, 1983.
8. W.F. Savage and A.H. Aronson, *Welding Journal*, (1966), p. 85s-89s.
9. M. Gremaud, M. Carrard and W. Kurz, *Acta Metallurgica et Materialia*, vol. 39, (1995) p. 1431-1443.

10. B. Majumdar, R. Galun, A. Weisheit and B. L. Mordike, *Journal of Materials Science*, vol. 32, (1997), p. 6191-6200.
11. G. Phanikumar, P. Dutta and K. Chattopadhyay, *Materials ageing and Life Management*, vol 3, Allied Publishers, Chennai (2000).
12. D. Brent, V. R. Voller, and K. J. Reid, *Numerical Heat Transfer*, 1988, vol. 13, pp 297-318.
13. G. Phanikumar, K. Chattopadhyay and P. Dutta, *International Journal of Numerical Methods in Heat and Fluid Flow*, (2001), (in press).
14. S. V. Patankar, *Numerical Heat transfer and fluid Flow*, Second Edition, Hemisphere Publications, New York, (1980).
15. G. Phanikumar, P. Dutta and K. Chattopadhyay, *Current Science*, 78, (2000), p. 847-849.
16. P. Dutta, Y. Joshi, and R. Janaswamy, *Numerical Heat Transfer A*, vol. 27, (1995), p. 499-518.